An update to this article is included at the end

Carbon 176 (2021) 458–469

Contents lists available at ScienceDirect

Carbon

journal homepage: www.elsevier.com/locate/carbon

# Shedding plasma membrane vesicles induced by graphene oxide nanoflakes in brain cultured astrocytes

Mattia Musto [a, 1], Pietro Parisse [b], Maria Pachetti [b], Christian Memo [a], Giuseppe Di Mauro [a], Belen Ballesteros [c], Neus Lozano [c], Kostas Kostarelos [c, d], Loredana Casalis [b, **], Laura Ballerini [a, *]

[a] International School for Advanced Studies (SISSA), 34136, Trieste, Italy
[b] ELETTRA Synchrotron Light Source, 34149, Basovizza, Italy
[c] Catalan Institute of Nanoscience and Nanotechnology (ICN2), Campus UAB, Bellaterra, 08193, Barcelona, Spain
[d] Nanomedicine Lab, National Graphene Institute and Faculty of Biology, Medicine & Health, The University of Manchester, Manchester, M13 9PT, United Kingdom

ARTICLE INFO

*Article history:*
Received 4 December 2020
Received in revised form
25 January 2021
Accepted 27 January 2021
Available online 8 February 2021

*Keywords:*
Graphene oxide
Extracellular vesicles
Atomic force microscopy and spectroscopy
FTIR-ATR and UVRR spectroscopy
Synaptic activity
Cortical neuronal cultures

ABSTRACT

Microvesicles (MVs) generated and released by astrocytes, the brain prevalent cells, crucially contribute to intercellular communication, representing key vectorized systems able to spread and actively transfer signaling molecules from astrocytes to neurons, ultimately modulating target cell functions. The increasing clinical relevance of these signaling systems requires a deeper understanding of MV features, currently limited by both their nanoscale dimensions and the low rate of their constituent release. Hence, to investigate the features of such glial signals, nanotechnology-based approaches and the applications of unconventional, cost-effective tools in generating MVs are needed. Here, small graphene oxide (s-GO) nanoflakes are used to boost MVs shedding from astrocytes in cultures and s-GO generated MVs are compared with those generated by a natural stimulant, namely ATP, by atomic force microscopy, light scattering, attenuated total reflection–fourier transform infra-red and ultraviolet resonance Raman spectroscopy. We also report the ability of both types of MVs, upon acute and transient exposure of patch clamped cultured neurons, to modulate basal synaptic transmission, inducing a stable increase in synaptic activity accompanied by changes in neuronal plasma membrane elastic features.
© 2021 The Author(s). Published by Elsevier Ltd. This is an open access article under the CC BY-NC-ND license (http://creativecommons.org/licenses/by-nc-nd/4.0/).

## 1. Introduction

In biology, newly described forms of intercellular communication comprise the release of vesicles, named extracellular vesicles, from virtually all cell types, including resident glial cells of the central nervous system (CNS), such as astrocytes and microglia [1,2]. In particular, the shedding of membrane vesicles is a recognized form of cross talk in the multidimensional signaling between astrocytes, (i.e. the majority of cells in the mammalian CNS), and neurons in physiology, but also in neurodegenerative and neuroinflammatory diseases as well as in brain tumors. Extracellular vesicle signaling molecules, either stored within their cargo or embedded in their plasma membrane, modulate relevant processes in the development, physiology and pathology of CNS target cells [3–6]. The signaling system based on release of extracellular vesicles comprises shedding microvesicles (MVs) and exosomes, characterized by different size, membrane composition, cargo and origin [7,8].

MVs are nanovesicles able to interact specifically with cells at local or distant sites [9]. In maintaining CNS functions, glial cells intensely communicate with neurons, also *via* the release of MVs, which represents a highly versatile tool to functionally impact the CNS [10–12]. MVs are considered a “vectorized” signaling system able to bind their target cells to transmit specific information. The

* Corresponding author.
** Corresponding author.
*E-mail addresses:* loredana.casalis@elettra.eu (L. Casalis), laura.ballerini@sissa.it (L. Ballerini).
[1] Present Addresses: Center for Synaptic Neuroscience, Istituto Italiano di Tecnologia (IIT), 16132, Genoa, Italy.

https://doi.org/10.1016/j.carbon.2021.01.142
0008-6223/© 2021 The Author(s). Published by Elsevier Ltd. This is an open access article under the CC BY-NC-ND license (http://creativecommons.org/licenses/by-nc-nd/4.0/).

reported spreading ability of MVs has suggested their potential exploitation as biomarkers or as engineered therapeutic carriers [13]. A comprehensive correlation between conditions used to release and harvest MVs from the same cell type, i.e. astrocytes, and their signaling ability, will impact our understanding of MVs physiology and the design of MV-based biomedical applications in the CNS [14,15]. Particular attention has to be conveyed to devise novel, cost-effective ways in generating MVs, in particular enhancing constitutive release.

Here, we concentrate on graphene oxide (GO), the most common derivative of graphene, whose properties can be tailored to adapt to new physical and biological applications [16,17]. GO flakes have been successfully designed for drug delivery applications in biomedicine [18]. In the CNS, small GO nano-flakes (s-GO) were shown to induce constitutive MV release from cultured astrocytes and to potentiate evoked MV release induced upon exposure to bzATP [19]. s-GO flakes, due to their physical features at the nanoscale, were reported to interfere with cellular membrane dynamics [19,20]. In addition, *via* adhesion to the plasma membrane, s-GO may alter the mechanical features of the lipid bilayer [21] triggering genuine biological responses, such as MVs signaling. Thus s-GOs may represent a tool to exploit mechanical signaling at the nanoscale to activate membrane release of MVs. Drug delivery applications where vesicle release from genetically engineered cells is required, may take advantage of the mechanical modulation of vesicle release brought about by graphene-based nanomaterials, representing a safer and cheaper alternative to pharmacological tools. Prolonged exposure to biomolecules able to induce MVs release, such as ATP, could in fact negatively affect cell physiology by promoting astrogliosis and inducing microglia-mediated neuroinflammatory responses [22].

We use the ability of s-GO to substantially increase the production of MVs from astrocytes to provide, for the first time, a robust and comparative vesicle characterization by means of ultramicroscopy, attenuated total reflection–fourier transform infra-red (FTIR-ATR) and UV Resonant Raman (UVRR) spectroscopy. We additionally explore by single cell patch-clamp recordings the impact of acute, local and transient delivery of MVs on neuronal basal synaptic activity and by atomic force microscopy (AFM) the accompanying changes in neuronal plasma membrane elastic features.

## 2. Material and Methods

### 2.1. Graphene oxide nanosheets synthesis

GO was manufactured under endotoxin-free conditions through our modified Hummers' method as previously described [19]. The complete characterization of the material used is shown and summarized in the Supplementary experimental section and Supplementary Figure S1 and Table S1.

### 2.2. Cell cultures

All experiments were performed in accordance with the EU guidelines (Directive 2010/63/EU) and Italian law (decree 26/14) and were approved by the local authority veterinary service and by our institution (SISSA-ISAS) ethical committee. All efforts were made to minimize animal suffering and to reduce the number of animals used. Animal use was approved by the Italian Ministry of Health, in agreement with the EU Recommendation 2007/526/EC.

Primary glial cultures were obtained from cortices isolated from neonatal rats (Wistar) at postnatal day 2–3 (P2–P3), as previously described [19,23]. Dissociated cells were plated into plastic 150 $cm^2$ flasks and incubated at 37 °C; 5% $CO_2$ in culture medium composed of DMEM (Invitrogen), supplemented with 10% fetal bovine serum (FBS; Thermo Fisher), 100 IU/mL penicillin, and 10 mg/mL streptomycin.

Cortical neurons were isolated from neonatal rat cortices (Wistar) at postnatal day 0–1 (P0–P1). Dissociated cells were then plated on poly-L-ornithine (Sigma) coated coverslips (Kindler, EU) at a concentration of 150000 cells in a volume of 200 μL and incubated at 37 °C; 5% $CO_2$ in a culture medium composed of Neurobasal-A (Thermo Fischer) containing 2% B27 (Gibco), 10 mM Glutamax and 0.5 μM Gentamycin (Gibco) for 8–10 *days in vitro* (DIV) before performing electrophysiological experiments.

### 2.3. MV isolation

MV shedding and isolation was performed as previously described [19]. One pool of MVs were collected from 21 to 24 DIV glial cultures previously treated with graphene oxide nanoflakes (s-GO) (10 μg/mL [19]), added to culture medium once and left for 6 days. At the end of 6-days exposure, the medium was removed and substituted with physiological saline solution, with the following composition: 152 mM NaCl, 4 mM KCl, 1 mM $MgCl_2$, 2 mM $CaCl_2$, 10 mM HEPES and 10 mM Glucose (pH adjusted to 7.4), at 37 °C and 5% $CO_2$ for 60 min prior to MVs collection and purification. The MVs pool was isolated from cultures treated (30 min) with benzoyl-ATP (bzATP; 100 μM) diluted in physiological saline solution. The 6-days exposure timepoint was chosen on the basis of previous Western blot experiments, and confirmed by our current experiments testing MVs release after 3 days of s-GO exposure (supplementary Figure S2) [19]. Negative controls were incubated with physiological solution without the presence of bzATP or s-GO. After the incubation period, cell medium was collected and centrifuged for 15 min at a speed of 300×*g* in order to remove cell debris. Supernatant was then collected and MVs were pelleted by centrifugation at 20000×*g* for 2 h. For $Ca^{2+}$ deprivation experiments, prior to supernatant collection and MVs pellet centrifugation, cultures were pre-incubated for 45 min in a saline solution identical to the physiological saline solution except for 0 mM $CaCl_2$, 3 mM $MgCl_2$ and 1 mM EGTA to allow the depletion of intracellular calcium storage. Upon this pre-treatment, we harvest the MVs from controls, s-GO treated and bzATP (30 min in $Ca^{2+}$ deprived solution; supplementary Figure S3).

### 2.4. Western blot analysis

MVs were prepared as previously reported, briefly they were resuspended in lysis buffer (50 mM Tris-HCl, pH 8.0, 150 mM NaCl, 1% NP40, 0.1% SDS), sonicated for 30 s, and then boiled at 95 °C for 5 min [19]. Samples were run on a 10% polyacrylamide gel and blotted onto nitrocellulose membranes (Millipore, Italy). Membranes were then blocked in PBS-Tween-20 (0.1%) plus 5% nonfat dry milk and incubated with the primary antibody antiflotillin-1 (dilution 1:1000) for 16 h at 4 °C. Membranes were then washed with PBS-Tween and incubated with peroxidase-conjugated anti-mouse secondary antibody (dilution 1:1000). Detection of immunolabeled ECL-exposed protein bands was measured with UVI-1D software over three independent experiments.

### 2.5. Immunofluorescence and confocal microscopy

Primary glial and cortical neurons cultures were fixed in 4% formaldehyde (PFA, prepared from fresh paraformaldehyde) in PBS for 20 min at room temperature (RT) and then washed in PBS. Free aldehyde groups were quenched in 0.1 M glycine solution for 5 min. The samples were permeabilized in 5% fetal bovine serum (FBS), 0.3% Triton-X 100 in phosphate buffer solution (PBS) for 30 min at

RT. Samples were then incubated with primary antibodies (mouse monoclonal anti-GFAP, Invitrogen, 1:500 dilution; rabbit polyclonal anti-β-tubulin III, Sigma-Aldrich, 1:500 dilution) diluted in PBS with 5% FBS at 4 °C for 1 h. Samples were then incubated with secondary antibodies (Alexa 488 goat anti-mouse, Invitrogen, 1:500 dilution; Alexa 594 goat anti-rabbit, Invitrogen, 1:500 dilution), and DAPI (Invitrogen, dilution 1:200) to stain the nuclei, for 45 min at RT and finally mounted on 1 mm thick glass coverslips using Fluoromount mounting medium (Sigma-Andrich). Images were acquired using a Nikon C2 Confocal, equipped with Ar/Kr, He/Ne and UV lasers with a 40 × or 60 × (1.4 NA) oil-objective (using oil mounting medium, 1.515 refractive index) to acquire glial cultures images and cortical neurons images respectively. 200 × 200 μm fields were acquired for cortical neurons images and 300 × 300 μm fields were acquired for glial cells images. Confocal sections were acquired every 0.25 μm for both the cultures.

### 2.6. Glial cell viability assay

Primary rat astrocytes (21–24 DIV) were exposed to s-GO 10 μg/mL or to equivalent volumes of the vehicle for 6 days. Cells were stained with propidium iodide (PI, 1 μg/mL; 15 min) for cell death quantification and subsequently fixed in PFA and labeled for DAPI for nuclei visualization and GFAP for visualizing astrocytes. The red (PI positive) fluorescent nuclei indicating dead cells were quantified at 40 × (1.4 NA) magnification using a Nikon C2 Confocal microscope, equipped with Ar/Kr, He/Ne and UV lasers, with random sampling of 10 fields per sample (n = 3 coverslips/sample, from 3 independent culture preparations). The average percentage of dead cells was calculated counting visual fields selected.

### 2.7. FM1-43 staining

Glial cells were incubated with the fluorescent styryl dye FM1-43 (2 μM) for 2 min in order to completely stain plasma membrane, then extensively washed with PBS and exposed for 30 min to bzATP (100 μM) or to standard saline solution [19]. Samples were placed in a recording chamber mounted on an inverted microscope (Nikon Eclipse Ti–U) and observed with a 40× objective (0.6 NA, PlanFluor, Nikon). Images (512 × 512 px) were acquired for 10 min with an exposure time of 150 ms (6.6 Hz) by a Hamamatsu Orca-Flash 4.0 digital camera controlled by an integrating imaging software package (HCImage, Hamamatsu). Recorded images were analyzed offline with the Clampfit software (pClamp suite, 10.2 version; Axon Instruments). Image time stacks were analyzed in selected regions of interest (ROI) to measure the variations in FM1-43 fluorescence intensity over time. Natural sample bleaching over time, due to prolonged light exposure, has the same time-course and intensity in all the three groups, as previously described [19].

### 2.8. Atomic force microscopy analysis

AFM characterization was performed as previously described [19]. Briefly, the pellet of MVs was re-suspended in PBS solution after isolation from cell cultures and a 15 μL drop of sample solution was placed and left to adsorb (30 min) onto a freshly peeled mica substrate. Vesicles were then fixed with 1% formaldehyde for 1 h (RT) in order to prevent their collapse during AFM acquisition. MVs were then washed with PBS and dried under a gentle stream of nitrogen. AFM analysis was performed in air at RT, using the semi-contact mode of a commercial instrument (Solver Pro, NT-MDT, RU). Silicon tips (NSC36/CR-AU, MikroMash, USA) with a typical force constant of 0.6 nN/nm and a resonance frequency of about 65 kHz were employed. Topographic height and phase images were recorded at 512 × 512 pixels at a scan rate of 0.5 Hz. Image processing was performed using Gwyddion freeware AFM analysis software, version 2.40. Diameter and height of each vesicle were evaluated from cross-line profiles, and results were statistically analyzed using Prism (Graphpad software).

### 2.9. Neuronal stiffness

9-10 DIV cortical neurons were exposed to MVs obtained by glial cultures treated with bzATP or s-GO and neuronal rigidity was assessed with AFM, 24 h after MVs exposure. Force spectroscopy measurements were performed with a commercial Smena AFM (NT-MDT, RU) mounted on an inverted microscope (Nikon Eclipse Ti–U). AFM cantilever deflection was measured when pushed against cortical neurons plated on a glass coverslip. Deflection values were subsequently converted into a force versus indentation curve based on cantilever spring constant and its displacement. Neuronal rigidity was evaluated in 50 randomly chosen neurons for each condition (from 3 independent experiments), acquiring three force spectroscopy curves in the center of each cell soma. The AFM tip was positioned by using an inverted microscope in bright field mode.

AFM micro-cantilevers with an elastic constant of about 0.03 nN/nm and a resonance frequency of about 10 kHz (CSG01 tipless cantilevers from NT-MDT, RU) were used. A borosilicate glass microsphere of about 18 μm in diameter (18.2 ± 1.0 mm from Duke Standards, CA, USA) was manually glued at the end of each cantilevers using a UV curable glue (Norland Optical Adhesive 61 from Norland Products Inc., NJ, USA). Force spectroscopy measurements were performed at a constant indentation speed of 1 mm/s with a maximum value of indentation deepness set at 500 nm. Elastic modulus values (E), expressed in kPa, were determined by fitting obtained force–indentation curves with a Hertzian model for the tip, using AtomicJ (v. 1.7.3) analysis software [24].

### 2.10. Nanoparticle tracking analysis (NTA)

Measurement and analysis of MVs size distribution by NTA was performed on a NanoSight LM10 system (Malvern) using approximately 500 μL of MVs of both conditions (bzATP-derived and s-GO-derived) diluited 1:20 in MilliQ $H_2O$. Individual videos of 60 s (recorded at 25 FPS; 3 videos per group) for each sample were acquired at RT using the maximum camera gain, a detector threshold equal to 8 and analyzed by the NanoSight particle tracking software to calculate size and vesicle concentration.

### 2.11. FTIR-ATR spectroscopy and UV Resonant Raman (UVRR) measurements

MVs were isolated from 21 to 24 DIV glial cultures by centrifugation as described above. MVs pellet was successively washed with NaCl solution (150 mM) and finally re-suspended in 50 μL of the same solution in order to avoid contribution of phosphate and sugar groups to the IR absorbance spectra. The IR measurements were carried out at the BL10.2-IUVS beamline at Elettra synchrotron Trieste. The spectra were collected in ATR mode using a MIR DLaTGS detector and a KBr-broadband beam-splitter. For each IR measurement, 2 μL of sample solution were spread over the whole area of a monolithic diamond ATR plate and left to dry forming a thin film. For each sample, 20 spectra were collected in the range 4000–800 $cm^{-1}$, accumulating 256 scans for each spectrum reaching a resolution of 4 $cm^{-1}$. Each spectrum was corrected for the background, aqueous vapor, $CO_2$ and not normalized to any absorbance band.

UVRR measurements were performed at the BL10.2-IUVS beamline at Elettra synchrotron Trieste using the experimental

set-up reported [25]. 5 μL of vesicles solution were drop-casted onto an aluminum foil, allowed to dry and kept under nitrogen purging. All the measurements were performed at RT, using an excitation wavelength of 244 nm and tuning the power of the incoming radiation to 50 μW. The outcoming radiation was collected in backscattering geometry by using a triple stage spectrometer (Trivista, Princeton Instrument) with a spectral resolution of 8 $cm^{-1}$. Samples were continuously oscillated horizontally in order to avoid photodamaging.

### 2.12. Electrophysiological recordings

Patch-clamp recordings (whole-cell, voltage clamp mode) were performed from visually identified (under differential interference contrast - DIC - microscopy) cortical neurons (DIV 8–10) placed in a recording chamber, mounted on an inverted microscope (Eclipse Ti–U, Nikon, Japan) and superfused with control physiological saline solution of the following composition (in mM): 152 NaCl, 4 KCl, 1 MgCl2, 2 CaCl2, 10 HEPES and 10 Glucose (pH adjusted to 7.4 by NaOH 1 M; osmolarity 300 mOsm). Cells were patched with glass pipettes (4–7 MΩ) containing (in mM): 120 K gluconate, 20 KCl, 10 HEPES, 10 EGTA, 2 $MgCl_2$ and 2 $Na_2ATP$ (pH adjusted to 7.35 by KOH; osmolarity 298 mOsm). All electrophysiological recordings were performed at RT and the spontaneous, basal synaptic activity was recorded by clamping the membrane voltage at −70 mV (corrected for liquid junction potential, which was −14 mV). To investigate the acute effect on synaptic activity of glia-derived MVs, an injection pipette (patch pipette with resistance of 1–4 MΩ) filled with MVs previously isolated glial cultures as described above and re-suspended in 100 μL of extracellular saline solution was positioned at 200 μm from the cell soma and connected to a pico-spritzer (PDES-02DX, npi Electronics) with 0.3 psi in-line pressure [19]. On the basis of MVs quantification obtained by NTA measurements, and considering that MVs isolation was performed using the same protocol in all the experiments described, we calculated that the concentration of MVs used for these tests was approximately of $6.64 \times 10^9$ for MVs obtained by bzATP stimulation and $1.64 \times 10^{10}$ for MVs isolated from s-GO treated cultures. Baseline spontaneous synaptic activity was recorded for the 10 min prior delivering the puff (500 ms duration) of MVs and followed up for 20 min to verify changes in post synaptic current (PSC) frequency and amplitude induced by the fusion of MVs with neuronal membranes.

Data were collected by Multiclamp 700B patch amplifier (Axon CNS, Molecular Devices) and digitized at 10 kHz with the pClamp 10.2 software (Molecular Devices LLC, USA). All recorded events were analyzed offline with the AxoGraph 1.4.4 (Axon Instrument) event detection software (Axon CNS, Molecular Devices).

### 2.13. Statistical analysis

Data sets found to follow a non-normal distribution, were represented as box plot. The central thick horizontal bar in the box plots indicates the median value, while the boxed area extends from the 25th to 75th percentiles with the whiskers ranging from the 2.5th to the 97.5th percentiles. Statistically significant differences between two non-parametric data sets were assessed by Mann-Whitney's test, while to assess statistically significant differences among three data-set we used the Kruskal-Wallis test and Dunn's post hoc test. $P < 0.05$ was considered at a statistically significant.

## 3. Results and discussion

Astrocytes were isolated from postnatal (2–3 days) rat (Wistar) cortices, as previously described [19,20,23]. We used visually homogenous s-GO dispersions containing s-GO nanosheets with lateral dimensions predominantly between 50 and 500 nm [19,20]. We treated pure glial cell cultures with s-GO (10 μg/mL) for 6 days [19]. Immunofluorescence labeling by antigen against glial-fibrillary acidic protein (GFAP), an intermediate filament protein that is highly specific for cells of the astroglial lineage, was used to visualize control and s-GO-treated neuroglial cultures (GFAP, in green; Fig. 1a) [26]. At the low concentrations used, s-GO treatment did not impair astrocyte morphology and cell density when compared with matched control cultures (box-plot in Fig. 1b) [19,27]. Viability of glial cells was confirmed by propidium iodide (PI) cell death assay. Control and s-GO treated cultures were incubated with PI, which stain dead cells nuclei (Fig. 1c, in red) and the percentage of PI-positive nuclei was calculated (bar plot in Fig. 1d). Graphene nanosheets cytotoxicity is a largely debated issue, due to the variable impact on cell toxicity of several material's features, related either on the GO physical-chemical properties (thickness, size, surface functionalization, aggregation state and concentration) or on the synthesis method [28,29], the experimental conditions adopted here and in our previous works [19,20] exclude any cytotoxic effect on glial cells or neurons, both *in vitro* and *in vivo*.

MVs are released into the extracellular space by direct budding from the plasma membrane of astrocytes [30]. To explore the dynamics of MVs release in control, in s-GO treated and in ATP treated (see below) astrocytes, we measured the presence of changes in membrane trafficking by briefly incubating cultures with the fluorescent styryl dye FM1-43 and then quantifying the astrocyte-membrane fluorescence decay to provide a cumulative measure of exocytosis in the different growth conditions [19,30].

FM dyes are fluorescent probes that reversibly stain membranes, and are largely used for optical real-time measurements of membrane dynamics and secretory processes [31–33]. Incubation with the FM dye (2 μM, 2 min) resulted in clear surface membrane staining of control, bzATP, an agent known to evoke massive MVs release (100 μM, 30 min) and s-GO treated cultures (10 μg/mL, 6 days), highlighted in Fig. 1e (left panels) [30]. Brighter spots were considered as adherent debris and were excluded from the analysis. Besides these, both bright and weak FM-stained plasma membrane domains were present along the whole cytoplasmic surface and became visible within 2 min incubation (Fig. 1e). Due to this initial variability in the intensity of the membrane staining, all FM de-staining measures were normalized to the relative time 0. Once astrocyte membranes were labeled by the fluorescent dye FM1-43 we measured the plasma membrane de-staining over a fixed time (10 min) in control, in s-GO treated cultures, or during acute exposure to bzATP, under the same culturing conditions [19]. Representative fluorescence intensity traces are shown in Fig. 1f (top plot); the dynamic of the fluorescence decay observed in control cultures, indicates the presence of physiological bleaching of fluorophore over the acquisition time course, however s-GO and bzATP groups, despite the same bleaching-induced loss of fluorescence, showed a faster de-staining rate in respect to controls. This is also visualized by the time-lapse images framed at time 0 s, 300 s and 600 s of the crude recordings (Fig. 1e middle and right panels). We quantified the fluorescence decay time constant ($\tau$) values (box plot of Fig. 1f) and detected shorter decay values in both bzATP and s-GO groups ($median_{control} = 219$ s; $median_{bzATP} = 184.2$ s; $median_{s\text{-}GO} = 163.9$ s). This result suggested that the membrane de-staining was actually related to MVs release, as expected in bzATP treated cells, more than to other membrane turnover activities. Such a release was comparable between bzATP and s-GO, both significantly faster than controls ($P_{bzATP} < 0.001$; $P_{s\text{-}GO} < 0.001$).

The release of MVs suggested by FM1-43 measures, was confirmed by immunoblot analysis for the biomarker flotillin-1 of

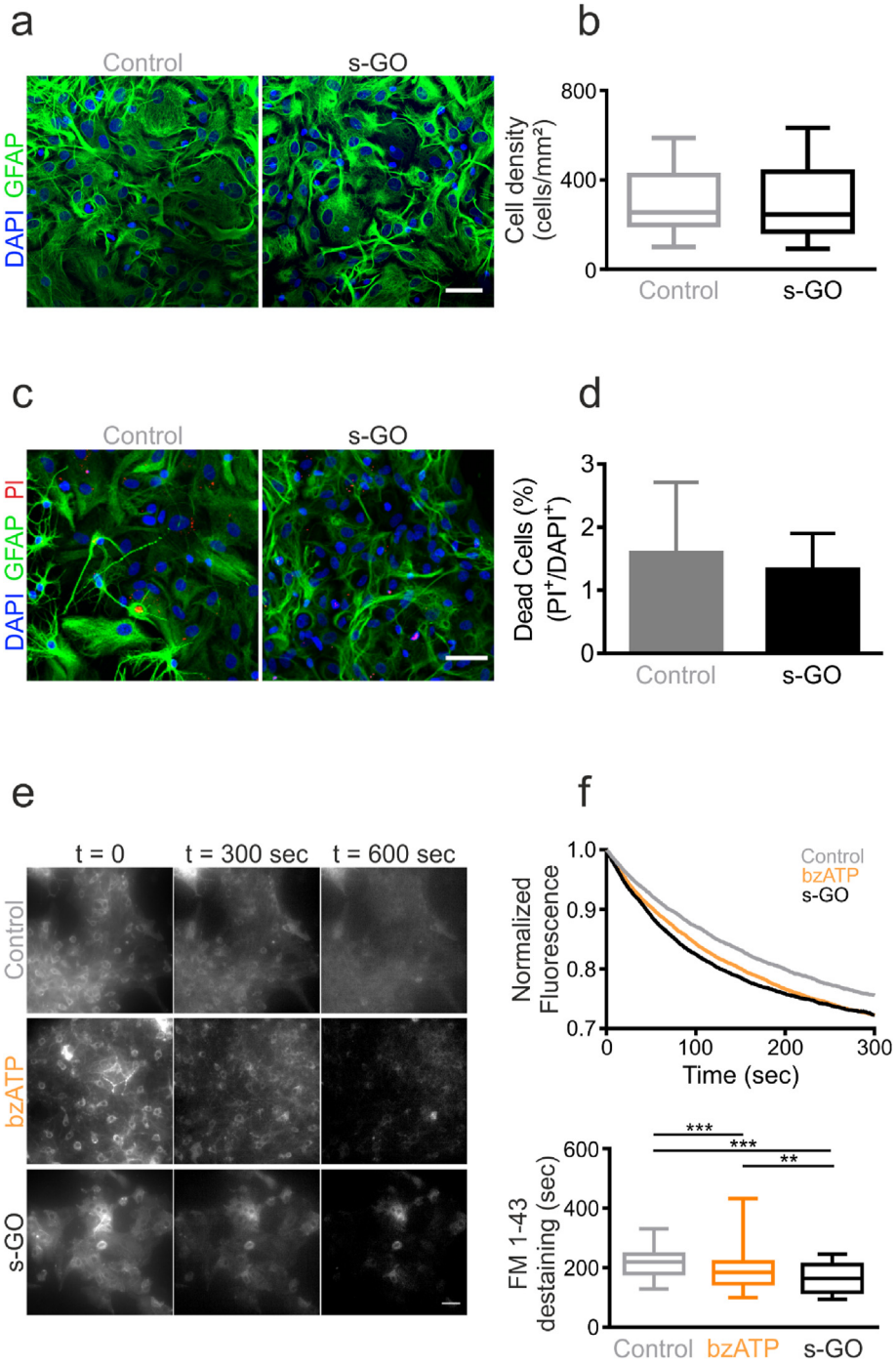


**Fig. 1. Graphene oxide nanosheets does not affect astrocytes vitality.** Cultured astrocytes release microvesicles (MVs) upon ATP or s-GO stimulation. a) Confocal images visualize cultured astrocytes in control and after s-GO (10 μg/mL; 6 days) treatment; anti-GFAP, in green, and DAPI (to visualize nuclei), in blue; scale bar 50 μm. b) Box plot summarizes the cell density measures; note the similar values in both groups. c) Confocal images visualize cultured astrocytes in control and after s-GO (10 μg/mL; 6 days) treatment. Cultures were treated with propidium iodide (PI) to visualize death cells. Anti-GFAP, in green, DAPI (to visualize nuclei), in blue and PI in red; scale bar 50 μm. d) Histogram summarizes the percentage of death cells followed the s-GO exposure and in control condition; note that there are no significant difference between two groups e) Surface membrane staining and activity dependent de-staining of FM1-43 in cultured astrocytes, scale bar 25 μm. f) Normalized FM1-43 de-staining traces (top) in control astrocytes (light grey), in bzATP treated once (orange) and in s-GO treated once (black). The box plot (bottom) summarizes the decay time constant $\tau$ of FM1-43 de-staining in the three conditions ($median_{control}$ = 219.2 s; $median_{bzATP}$ = 184.2 s; $median_{s\text{-}GO}$ = 163.9 s). Thick horizontal bars in the box plots indicate median value; boxed area extends from the 25th to 75th percentiles, whiskers from 2.5th to the 97.5th percentiles. Significance: **P < 0.01 ***P < 0.001, Kruskal-Wallis test, Dunn's post hoc test). (A colour version of this figure can be viewed online.)

the supernatant collected from control and treated cultures (Fig. 2a). As expected, bzATP stimulation and s-GO incubation induced the appearance of a thick band corresponding to flotillin-1 (Fig. 2a), a signature of MVs release by astrocytes, with an additive effect between s-GO exposure and pharmacological stimulation with bzATP ($s\text{-}GO_{Ringer}$ is quantified as 100% more than $Control_{Ringer}$; $bzATP_{Ringer}$ is quantified as 360% more than $Control_{Ringer}$; $bzATP_{s\text{-}GO}$ is quantified as 2900% more than $Control_{Ringer}$. Calculated over three independent experiments) [19,30,34]. In control conditions only a weak band was perceived, indicating that MVs

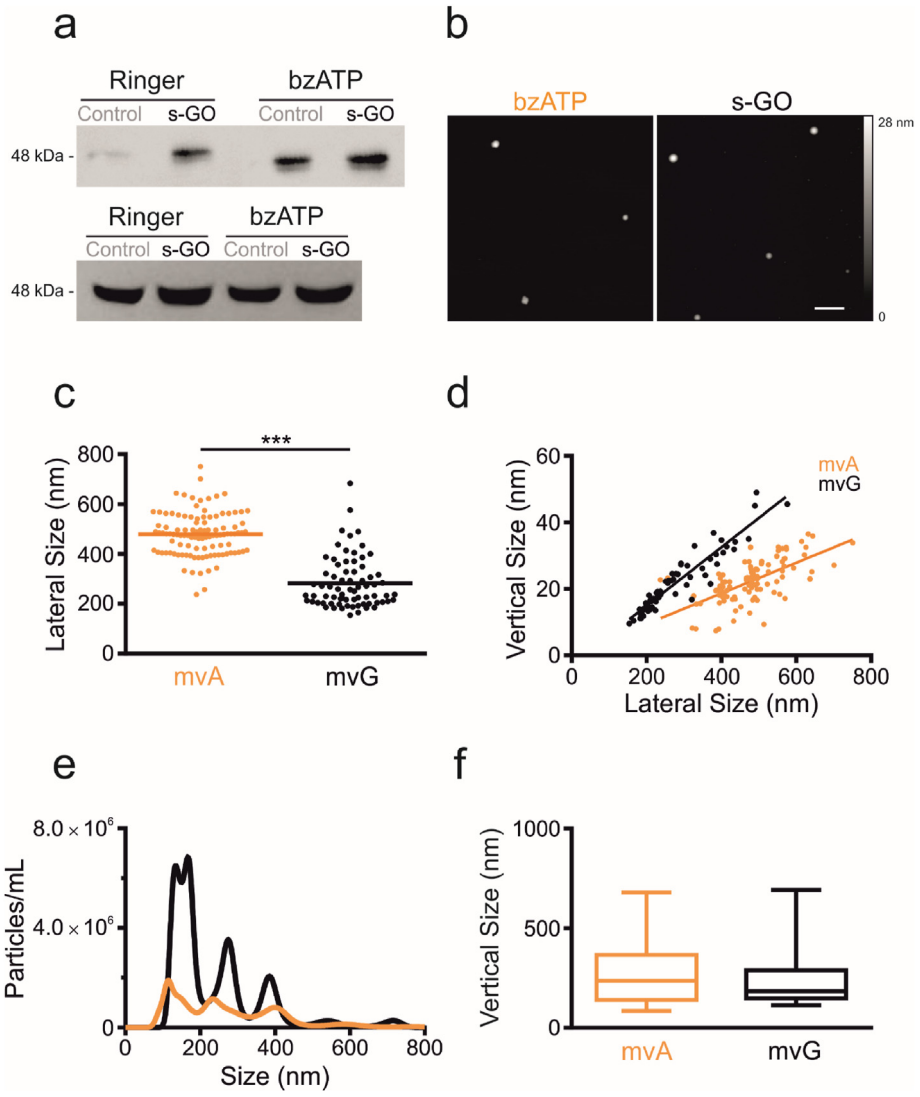


**Fig. 2. Graphene oxide nanosheets and bzATP induce MVs release in Astrocytes.** Microvesicle released by glial cells *via* bzATP or s-GO stimulations characterized by ultra-resolution approaches. a) Western blotting of the pellets (top row) and cell lysates (bottom row) for the MV marker flotillin-1 (N = 3). Pellets were obtained from the medium of glial cultures treated or untreated (control) with s-GO under two different conditions: not stimulated (ringer) or stimulated (bzATP) by 100 μM bzATP. $s\text{-}GO_{Ringer}$ is quantified as 100% more than $Control_{Ringer}$; $bzATP_{Ringer}$ is quantified as 360% more than $Control_{Ringer}$; $bzATP_{s\text{-}GO}$ is quantified as 2900% more than $Control_{Ringer}$. Calculated over three independent experiments. b) AFM topographic reconstruction of MVs isolated from cultured primary astrocytes treated with bzATP (100 μM) and s-GO (10 μg/mL) and performed in air (semi-contact mode). Scale bar 500 nm. c) Lateral size values distribution and median values for both groups, note that mvG lateral size is significantly smaller than that of mvA ($median_{mvA}$ = 479 nm; $median_{mvA}$ = 244.1 nm; ***P > 0.001, Mann-Whitney test). d) AFM measures of lateral size are plotted against AFM measures of height of MVs isolated from glial cells treated by bzATP (100 μM; mvA; in orange) or by s-GO (10 μg/mL; mvG; in black). e) Size distribution of MVs isolated from glial cells treated by bzATP (100 μM; in orange) or by s-GO (10 μg/mL; in black) measured by nanoparticle tracking analysis (NTA). Values of the peaks are expressed in nm. f) Lateral size values distribution and median values for both groups, obtained by NTA measurement. (A colour version of this figure can be viewed online.)

constitutive release in culture was poorly detectable. Atomic force microscopy (AFM) topographic reconstruction of re-suspended MVs pellet (Fig. 2b) confirmed the presence of MVs detected by the immunoblot in both bzATP (mvA) and s-GO (mvG) groups. When investigating the effect of shorter (3 days) exposure to s-GO, Western blot experiments (supplementary Fig. S2) showed the absence of a significant increase in MVs constitutive release when compared to control. Yet, bzATP release of MVs was potentiated by 3 days s-GO (supplementary Fig. S2) suggesting that s-GO already modulated MVs release, but longer time of s-GO exposure are needed to enhance basal release in the absence of additional stimuli. In an additional set of Western blot experiments, we tested the sensitivity of bzATP and s-GO MVs release to extracellular calcium deprivation (supplementary Fig. S3). Differently from bzATP, s-GO release was apparently not affected by calcium removal. In control condition, a thick band appeared upon calcium removal, suggestive of an increase in constitutive release (supplementary Fig. S3). These preliminary results hint at release mechanisms differently tuned by calcium among control, bzATP and s-GO and require further studies.

We systematically investigated and compared the MV size distribution by means of AFM and nanoparticle tracking analysis (NTA) measurements. AFM images show the presence of roundish protrusions of dimensions compatible with the size of MVs. No other kind of contaminant was present, to indicate that the procedure for isolating and collecting MVs from the medium was clean and effective. When analyzed by AFM (Fig. 2c) s-GO-derived MVs (mvG) lateral size were significantly smaller (n = 72, $median_{mvG}$ = 244 nm) than bzATP-derived ones (mvA; n = 107, $median_{mvA}$ = 479 nm) (P < 0.001). Conversely, we detected no

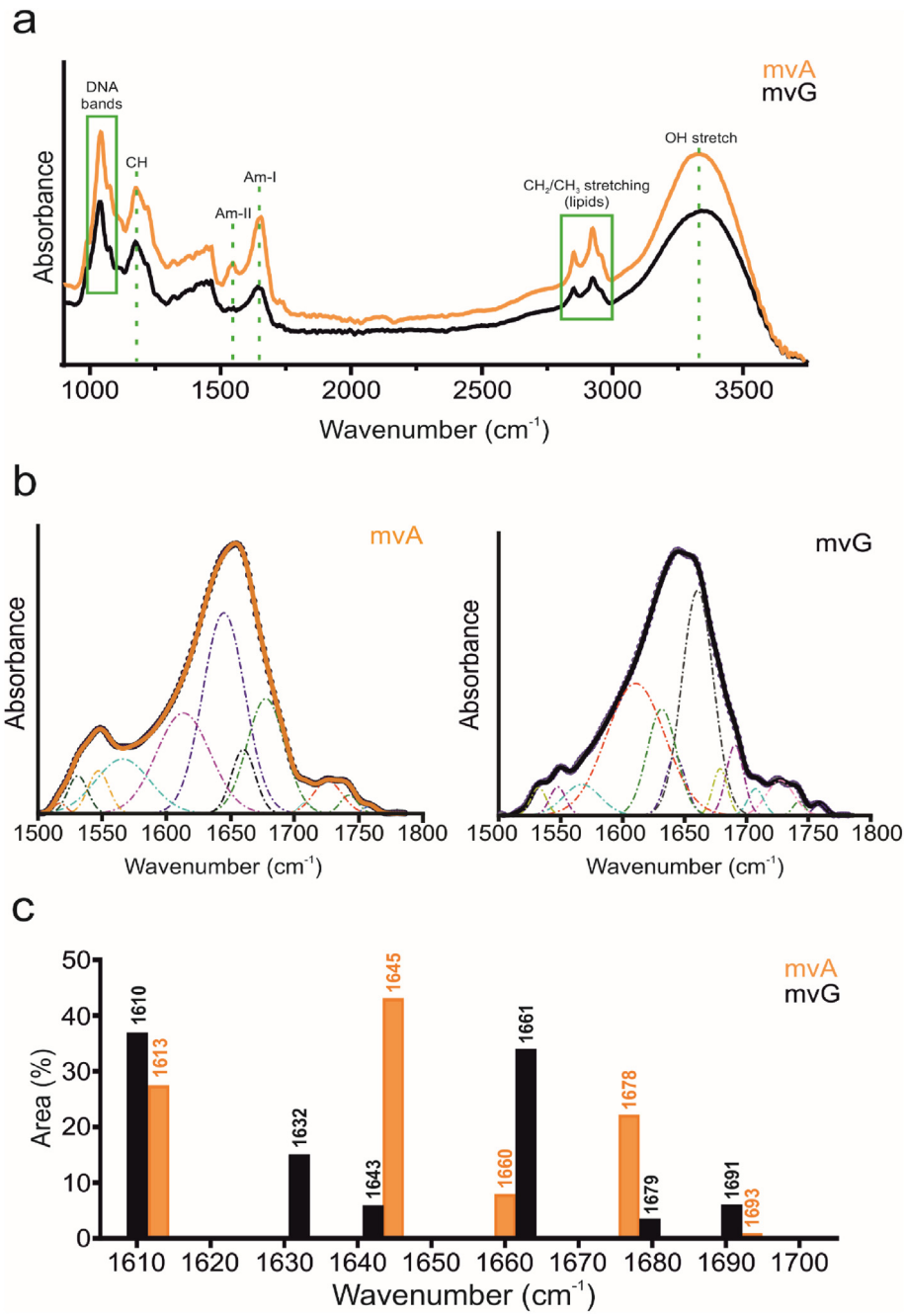


**Fig. 3. MVs characterization by infrared spectroscopy.** Microvesicles produced by glial cells *via* bzATP or s-GO stimulation and characterized by infrared spectroscopy. a) Infrared spectra of microvesicles obtained by bzATP stimulation (mvA, in orange) or by s-GO exposure (mvG, in black) in the region 950-3600 $cm^{-1}$. Contributions arisen from nucleic acids, proteins and lipids characterize the spectra. The two boxes in green and the green dashed lines are used as eye-guides to highlight nucleic acids, $CH_2$–$CH_3$ stretching of lipids and protein amide bands, respectively. b) Fitting procedure applied to mvA (on the left) and mvG (on the right) amide bands spectra. Multicomponent Gaussian curves were used to actually reproduce the experimental data. The centres of the Gaussian curves were chosen as the minimum of the 2nd derivative of the spectrum and kept free to variate within 4 $cm^{-1}$ around its maximum. c) Histograms representing the areas of the Gaussian curves used to reproduce the experimental data of mvA (in orange) and mvG (in black) in the region 1500-1785 $cm^{-1}$. The areas of each band has been weighted respect to the total amide band area which they belongs to (i.e. 1640 $cm^{-1}$ band has been weighted with respect to the total Am–I band area). (A colour version of this figure can be viewed online.)

differences in MV height values ($median_{mvG}$ = 19 nm; $median_{mvA}$ = 22 nm; P = 0.17). Within each group, the distribution of size values detected was not negatively correlated to the height, as shown in Fig. 2d (left; $r_{mvG}$ = 0.8808 and $r_{mvA}$ = 0.4039; P < 0.001). However, AFM experiments were performed in air, thus a not specific flattening of MVs caused by vesicle collapsing might have influenced these measurements. In principle differences in MV elastic properties, potentially related to diverse membrane components, might lead to a variable collapsing of MVs when measured in air.

Since AFM measurements are affected by the reduced size of the analyzed samples, and might not reflect the entire MVs population, we decided to use nanoparticle tracking analysis (NTA) to perform bulk analysis of vesicles in aqueous suspension. NTA tracks single particle Brownian motion within a dark field microscope, derives mean square vesicles velocity and translates them into size distribution [35]. NTA revealed a more complex pattern of size

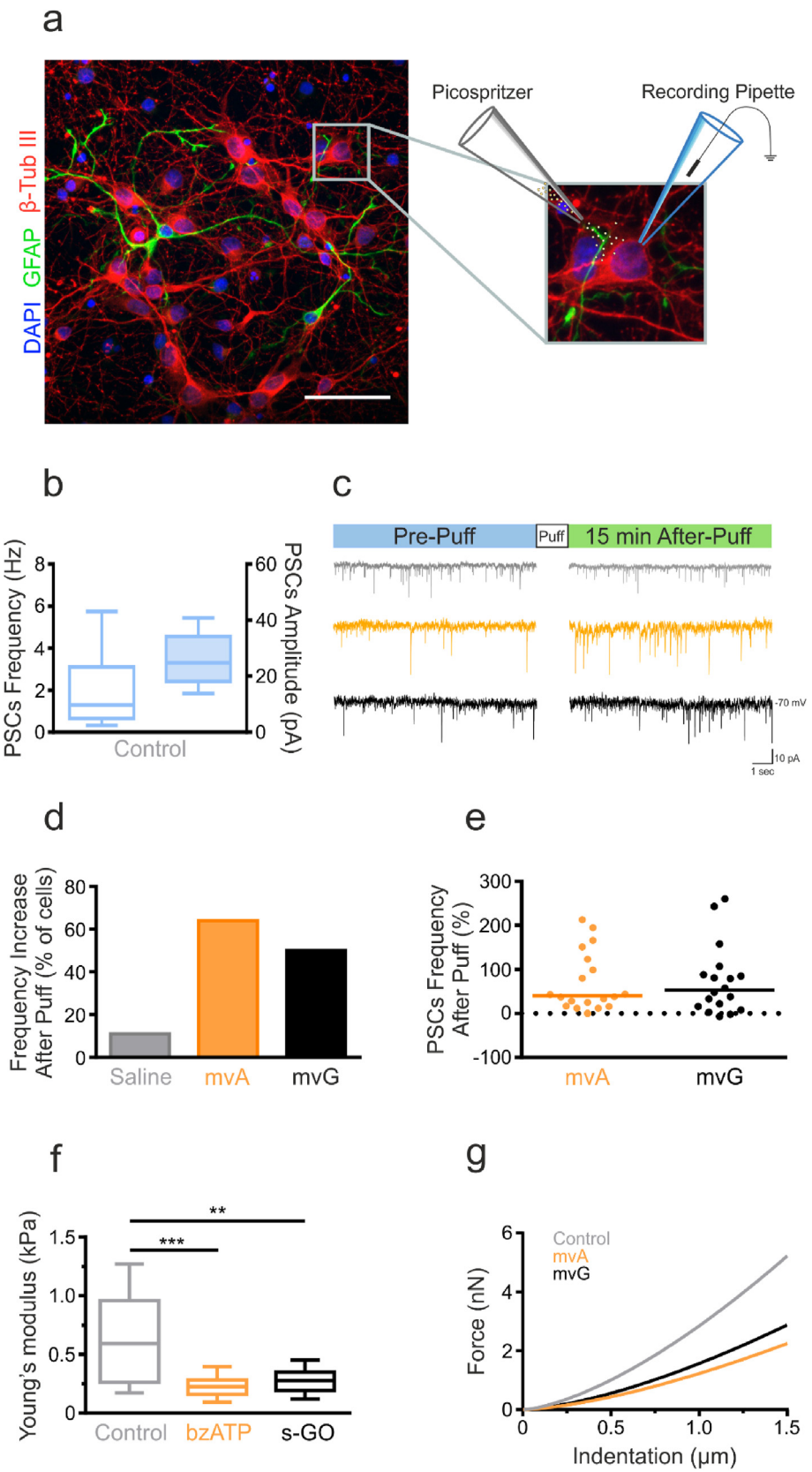


**Fig. 4. MVs released by astrocytes affect cortical neuron post-synaptic activity and mechanical properties.** Potentiation of synaptic activity upon local applications of MVs in cortical neurons. a) Confocal micrograph visualizing cortical primary cultures at 8 days *in vitro*; anti-class III β-tubulin is used to visualize neurons (in red), anti-GFAP for astrocytes (in green) and DAPI (in blue) to visualize neurons. Scale bar 50 μm. On the right, a representation of the experimental setting for the simultaneous MVs pressure-release (*puff*) and the cell patch-clamp recording from cultured neurons. b) Box plot summarizes the PSCs frequency and amplitude values in control cortical neurons. c) Top: diagram of the experimental protocol. Bottom: representative current tracings of the spontaneous synaptic activity detected prior and after puff applications of control saline (in light grey) or mvA

distribution (Fig. 2e): in the case of mvA we observed three subpopulations of vesicles at 115 nm, 235 nm and 400 nm respectively while in the case of mvG we found two partially overlapping peaks at 135 nm and 168 nm, plus two distinct peaks at 275 nm and 385 nm (Fig. 2e). The diameter analysis revealed a slight, but not significant, difference between the two populations with the diameter of mvG smaller and less distributed, compared to those of mvA ($median_{mvA}$ = 235.4 nm; $median_{mvG}$ = 183.6 nm) (Fig. 2f). These results convincingly suggested a comparable size distribution in both MV populations and subpopulations. However, we detected a significant difference in the number of vesicles released within the same time window (Fig. 2e) to indicate that cultures treated with s-GO produced more MVs when compared to cultures stimulated with bzATP (mvA = $3.32 \times 10^8$ vesicle/mL; mvG = $8.19 \times 10^8$ vesicles/mL), consistently with our results obtained by MV release analysis and immunoblot (but see also Visnovitz et al., 2019 [36]). Therefore, even though the overall size of the MV population produced did not change, s-GO was more efficient in generating MVs from astrocytes.

In order to analyze the macromolecular composition of MVs we took advantage of two complementary techniques: FTIR-ATR and UVRR spectroscopy. For these measurements, MVs were isolated by differential centrifugation as described before (see Material and Methods). To avoid any spurious effect due to the absorption of phosphate groups from the buffer, we washed and re-suspended the MVs pellet with a NaCl solution (150 mM). The infrared (IR) absorbance spectra (Fig. 3a) revealed a clear contribution of the CH and the phosphate bands linked to DNA in both samples, mvA and mvG, as well as the lipid signatures at 2900-3000 $cm^{-1}$, arisen from the $CH_2$ and $CH_3$ stretching mode. The amide I and amide II bands between 1500 and 1785 $cm^{-1}$, the two major protein bands in the IR spectrum, show more pronounced differences between the two populations of vesicles. The amide I band, which is primarily related to the C═O stretching in the peptide bonds and modulated by the proteins' secondary structures, displayed similar shapes for mvA and mvG. The amide II band, primarily due to C–N stretching and N–H in plane bending vibrations, also reflecting the protein secondary structure, was instead clearly depleted in the case of mvG. To gain insights into the contribution of different protein secondary structures in the two families of vesicles, we analyzed the second derivative of the IR signal in the amide I + amide II region (Fig. 3b) and used the position of the minima to guide a multicomponent gaussian fit of the bands in the region 1500 and 1785 $cm^{-1}$. The % area contributions obtained by the fit are reported in Fig. 3c. The low-energy flank of amide I of both mvA and mvG is characterized by the presence of the 1610-1613 $cm^{-1}$ vibrational peak which could be addressed to a mixed contribution arisen from β-sheets and side-chains vibrations. Additionally, the band at 1660 $cm^{-1}$ might also be derived from the presence of RNA in the vesicles [37]. Noteworthy, the relative populations of the peaks at approximately 1645 $cm^{-1}$, 1660 $cm^{-1}$ and 1678 $cm^{-1}$ are inverted between mvA and mvG. According to the literature [37], the 1645 $cm^{-1}$ peak (depleted in mvG) might be assigned to random structures and/or helices; the 1660 $cm^{-1}$ peak (depleted in mvA) to flexible helices (as $3_{10}$ helices); the 1678 $cm^{-1}$ peak (depleted in mvG) to beta structures such as b-turns. The bands at 1632 $cm^{-1}$ and at 1693 $cm^{-1}$, both present in the mvG only, are ascribed to antiparallel beta sheet, as found in aggregates in tissues [37,38]. We can conclude that mvGs contain proteins with perturbed secondary structure, characterized by beta structure-based aggregates and flexible helices. No significant variations in the DNA phosphate bands were measured as well as the nature or localization of the DNA signature detected. It is interesting to note that in previous measures the DNA delivered by EVs has been reported to be stocked either inside the vesicles or on their surface [39].

UV Resonant Raman (UVRR) measurements taken using an excitation wavelength of 244 nm (see experimental section and supplementary Fig. S4) confirmed the amide I signal depression in mvG absorption spectrum. Due to an overlap between the UVRR s-GO band, we could not confirm or discard the presence of s-GO inside the vesicles. Thus, we cannot exclude that the changes in protein native structure might be due to s-GO altering the MV micro(nano)environment or the possibility of a general interference with the measurements. The absence of astrocytes cytotoxicity, even upon prolonged exposure to s-GO, together with the functional measures of increased MVs release kinetic obtained by live imaging, are against a mere alteration in protein integrity due to denaturation of membrane proteins in the presence of s-GO [40–42]. FTIR-ATR spectroscopy is a powerful tool to assess the disordered character of proteins, and the absence of a well-defined structure under native conditions is a peculiar property of intrinsically disordered proteins (IDP) [43,44]. In this framework, IDPs might represent a specific signal vehiculated by mvG and the lack of protein structural constraints could facilitate several, yet unknown, biological processes [44].

It is clearly visible that mvA and mvG vesicles have a different secondary structure: the former is mainly characterized by an intense peak at 1645 $cm^{-1}$ (43%), which can be assigned to random structures/a-helix structure, and at 1678 $cm^{-1}$ (22%) usually assigned to b-turn and at 1613 $cm^{-1}$ (27%), which could be assigned to side chains vibrations; in contrast, mvG are mainly characterized by anti-parallel b-sheets structure (1632 (15%) and 1693 $cm^{-1}$ (3%) bands) with a strong contribution of flexible 3–10 helix (1661 $cm^{-1}$ peak (34%)) and of side chain band at 1610 $cm^{-1}$ (37%).

Finally, we set up a functional test to compare the impact of mvG delivery with that of mvA on synaptic activity, when neuronal networks are acutely and transiently exposed to MVs. To this aim, we isolated cortical neurons and glial cells from postnatal rat cortices and cultured them for 10 days. Fig. 4a shows confocal high magnification microscopy images of cortical cultures where neurons were visualized by labeling class III β-tubulin (in red), a microtubule component expressed exclusively by neurons, while astrocytes were visualized by GFAP labeling (in green) [45]. We patch-clamped visually identified cortical neurons (in voltage clamp configuration, holding potential − 70 mV), while a second pipette for the local delivery of saline solution was positioned at a distance of 200 μm (under microscopy visual control) from the recorded cell (sketched in Fig. 4a, right). We estimated that, at this distance, the application of a brief (500 ms) pulse of pressure should result in a local (i.e. on the recorded neuron) and transient delivery of standard saline solution alone or containing mvG or mvA (re-suspended in saline). A typical feature of these cultures is the prominent expression of spontaneous synaptic activity, represented by heterogeneous postsynaptic currents (PSCs) of variable frequency and amplitude (box plots in Fig. 4b). Baseline PSCs were recorded before (10 min) and after (15 min) the local saline, mvG or

(in orange) or mvG (in black). d) Bar plots of pooled data summarize the % of cells displaying PSCs frequency increase upon delivery of pressure ejected saline (light grey), mvA (orange) and mvG (black). Note that in control (saline) the large majority (88%) of neurons did not increase their basal activity. e) The plot summarizes the distribution of the % of increase in PCSs frequency detected within the three groups. f) Elastic moduli of cortical neurons, grown on glass, and exposed to MVs isolated from glial cells previously treated with bzATP (orange) or s-GO flakes (black). Neurons treated with mvA and mvG are significantly less rigid if compared with control ($P_{mvA} < 0.001$; $P_{mvG} < 0.01$). Thick horizontal bars in the box plots indicate median value; boxed area extends from the 25th to 75th percentiles, whiskers from 5th to the 95th percentiles. Significance: **P < 0.01 ***P < 0.001, Kruskal-Wallis test, Dunn's post hoc test) **g.** Indentation curves of cortical neurons previously treated with mvA or mvG. (A colour version of this figure can be viewed online.)

mvA ejection. Fig. 4c shows representative current tracings where standard saline was pressure ejected (light grey, top), or where mvA solution (orange, middle) and mvG (black, bottom) were administered.

Since spontaneous fluctuations in PSCs frequency ≤15% of baseline values were frequently detected, we took this as the threshold value to estimate changes when comparing PSCs before and after pressure ejections of saline. In the large majority (88%, n = 16/18 neurons; histograms in Fig. 4d) of neurons exposed to saline solution alone, spontaneous PSCs frequency did not change. On the contrary, within 5–8 min from the acute mvA and mvG ejections, PSCs frequency was stably increased in 64% (n = 16/25 neurons, mvA) and 54% (n = 13/24 neurons, mvG; summarized in the histograms of Fig. 4d) of recorded neurons. Fig. 4e shows the increases in PSCs frequency in individual experiments and highlights the variability of such changes when administering MVs, with increased frequencies ranging from 25% to 200%. Since we could not experimentally control the amount of MVs collected by primary astrocytes and delivered by pressure ejection, neurons were exposed to different amounts of MVs and this can in part explain the detected variability. PSCs frequency increases due to MVs exposures were not reversible upon 20 min washout. From such functional investigation, glial-signaling generated by ATP or s-GO affected similarly neuronal synapses upon transient, direct exposure.

To our knowledge, this is the first time that the functional effects of MVs generated by astrocytes on synaptic activity upon local delivery have been electrophysiologically documented. Neuroglia extracellular vesicles have been described to provide support on synaptic activity, with the majority of studies focused on microglia and inflammation, apparently regulating neural transmission at the pre-synaptic level [5,46–48]. Astrocytic MVs have been proposed to exert neuroprotective effects in neuropathology and in physiology, however the role of astrocytes or of discrete astrocyte populations in delivering different messages *via* MV release has yet to be elucidated [49,50].

After assessment of the ability of MVs released by glial cells to affect cortical neuron physiology within min after their interaction with the targeted neuron, we asked if the presumed fusion of vesicles with neuronal plasma membrane could also affect their mechanical properties. To investigate this aspect, we delivered MVs obtained from glial cultures previously treated with bzATP or s-GO to cortical neurons by re-suspending the isolated MVs in 100 μL of neuronal culture medium and adding them to neuronal cultures. 24 h after the exposure, force spectroscopy measurement on treated neuronal cultures were performed with AFM by positioning the tipless cantilever with a borosilicate glass bead previously glued on it [51], at the center of randomly chosen neurons. As showed by the boxplot in Fig. 4f, the exposure to mvA caused a significant softening of neuronal soma, when compared to controls ($median_{mvA} = 0.22$ kPa, $median_{control} = 0.59$ kPa; $P_{mvA} < 0.001$). A similar result was observed also in the case of mvG exposure even if the effect exerted on neuronal stiffness is less pronounced than that induced by mvA ($median_{mvG} = 0.28$ kPa, $median_{control} = 0.59$ kPa; $P_{mvG} < 0.01$). The reported effect of mvA and mvG on neuronal cell mechanical properties is presumably a consequence of vesicular fusion with the cellular plasma membrane, which may affect its lipid composition. Since the mechanical properties of a cell are mostly defined by plasma membrane features and the ones of the underlying cytoskeleton, a change in neuronal plasma membrane lipid composition can partially justify the observed reduction in mvA and mvG-treated neurons stiffness [52]. In particular, glia-derived MVs are able to transport the enzyme Acid sphingomyelinase (A-SMase) involved in the metabolism of sphingomyelin (SM), a precursor of the phospholipid sphingosine (sph). Sph and its metabolites have been already reported to play a fundamental role in facilitating synaptic vesicles release by changing the membrane composition at pre-synaptic level [48,53]. This intrinsic capacity of MVs to participate in membrane lipid metabolism may therefore modulate the contribution of plasma membrane to neuronal rigidity. In this context, the slight difference of stiffness values reported among mvA and mvG-treated neurons, although not statistically significant ($P_{mvA\text{-}mvG} > 0.05$) should not be underestimated [54,55]. It is tempting to speculate that this difference can be explained by the presence of specific proteins in the vesicles, that are unstable in mvG. Based on our measures, we cannot exclude the presence of residual s-GO flakes either inside or on the vesicle surface. It is known that GO is reportedly able to interact with the hydrophobic region of biological and model lipid membranes, even though the nature of the interaction is strictly dependent to its size and degree of surface oxygenation [56,57]. Assuming that the GO nanosheets, once added to the culture medium, can adsorb on plasma membrane or pierce it and being embedded in the lipid bilayer, there is a concrete possibility that MVs, which directly originate from plasma membrane, can include those flakes in their structure [30]. The horizontal transfer of s-GO from glial cells to cortical neurons, mediated by MVs, may therefore affect plasma membrane rigidity of targeted neurons. Regardless of this, we can exclude a direct effect of s-GO in synaptic transmission, reported to be transient and reversible upon acute exposure, in view of the persistent modulation of synaptic current frequency brought about by MVs [19,20].

## 4. Conclusion

Astrocyte-derived MVs may play significant roles in propagating signaling molecules, in CNS physiology and disease. Despite the increasing knowledge on extracellular vesicles (in particular exosomes) ability to promote inflammation or contribute in spreading of pathogenic proteins in neurodegenerative disorders (from Amyotrophic Lateral Sclerosis to Alzheimer disease [58,59]) little is currently known on their properties (mechanical, biochemical, lipid membrane composition, cargo nature etc.), in particular when focusing on the smaller class of such natural vectors, the MVs. Nevertheless, MVs emerge as key players in neuronal and synaptic physiology, able to influence neurotransmission, or to support neurons [48,60–62]. In our study, we report the ability of artificially generating MVs by s-GO transient exposure. MVs generated by s-GO were apparently characterized by altered protein content when compared to the ATP-driven ones. Intriguingly, the tuning of synaptic activity by mvG or mvA was similar, supposedly being related to features diverse from MV protein content. The ability of s-GO to interfere with exo-endocytotic membrane dynamics is not surprising, indeed we have described the ability of s-GO nanoflakes to interfere with presynaptic vesicle release *in vitro* and *in vivo* [19,20]. In the current work, we describe the direct interference of MVs with synaptic activity, presumably due to MVs fusion with the target neuron plasma membrane. Such an approach holds the potential to open new opportunities in engineering MVs for synaptic targeting. In this framework, it is tempting to speculate that s-GO interactions with the cell membrane mimic extracellular mechanical signaling at the nanoscale sufficient to enable the release of MVs, thus representing unconventional tools to exploit the physics governing vesicle release. We feel pertinent here to consider the fact, that the enormous potentiality of graphene-based materials in nanomedicine has already promoted the development of new generation-nanocarriers for either gene or drug delivery [17,63]. In this framework, we may speculate on future developments where engineered cells are mechanically induced to release MVs, carrying GO nanoflakes properly functionalized to deliver genes or drugs of interest and thus representing either the trigger and the cargo.

## Author contributions

M.M. performed cell biology, electrophysiology, and immunofluorescence experiments and analysis; M.M. and P.P. designed and performed AFM experiments; M.P. performed IR and UVRR experiments and analysis. CM and GDM performed biology and WB experiments; N.L. and K.K. contributed to the synthesis and characterization of thin graphene oxide of biological grade. BB performed SEM micrographs of GO. L.B. and L.C. conceived the study; L.B. conceived the experimental design and contributed to the analysis of data; L.B. wrote the manuscript.

## CRediT authorship contribution statement

**Mattia Musto:** Formal analysis, performed cell biology, electrophysiology, and immunofluorescence experiments and analysis, designed and performed AFM experiments. **Pietro Parisse:** designed and performed AFM experiments. **Maria Pachetti:** Formal analysis, performed IR and UVRR experiments and analysis. **Christian Memo:** performed biology and WB experiments. **Giuseppe Di Mauro:** performed biology and WB experiments. **Belen Ballesteros:** performed SEM micrographs of GO. **Neus Lozano:** contributed to the synthesis and characterization of thin graphene oxide of biological grade. **Kostas Kostarelos:** contributed to the synthesis and characterization of thin graphene oxide of biological grade. **Loredana Casalis:** conceived the study. **Laura Ballerini:** Writing - original draft, conceived the experimental design and contributed to the analysis of data, wrote the manuscript.

## Declaration of competing interest

The authors declare no competing financial interest.

## Acknowledgment

We acknowledge the financial support from the European Union's Horizon 2020 Research and Innovation Programme under grant agreement no. 785219 and no. 881603 Graphene Flagship. MM, PP and LC acknowledge CERIC-ERIC proposal grant n. 20167063 for the IR measurements, performed at the SISSI-Bio beamline of Elettra Sincrotrone Trieste. PP and LC acknowledge also the European Regional Development Fund and Interreg V-A Italia-Austria 2014–2020 project EXOTHERA (ITAT1036).

## Appendix A. Supplementary data

Supplementary data to this article can be found online at https://doi.org/10.1016/j.carbon.2021.01.142.

## References

[1] D.A. Shifrin, M.D. Beckler, R.J. Coffey, M.J. Tyska, Extracellular vesicles: communication, coercion, and conditioning, Mol. Biol. Cell 24 (2013) 1253–1259, https://doi.org/10.1091/mbc.e12-08-0572.
[2] Y.J. Yoon, O.Y. Kim, Y.S. Gho, Extracellular vesicles as emerging intercellular communicasomes, BMB Rep 47 (2014) 531–539, https://doi.org/10.5483/BMBREP.2014.47.10.164.
[3] V. Zappulli, K.P. Friis, Z. Fitzpatrick, C.A. Maguire, X.O. Breakefield, Extracellular vesicles and intercellular communication within the nervous system, J. Clin. Invest. 126 (2016) 1198–1207, https://doi.org/10.1172/JCI81134.
[4] C.P.-K. Lai, X.O. Breakefield, Role of exosomes/microvesicles in the nervous system and use in emerging therapies, Front. Physiol. 3 (2012) 228, https://doi.org/10.3389/fphys.2012.00228.
[5] V. Budnik, C. Ruiz-Cañada, F. Wendler, Extracellular vesicles round off communication in the nervous system, Nat. Rev. Neurosci. 17 (2016) 160–172, https://doi.org/10.1038/nrn.2015.29.
[6] A. Grimaldi, C. Serpe, G. Chece, V. Nigro, A. Sarra, B. Ruzicka, M. Relucenti, G. Familiari, G. Ruocco, G.R. Pascucci, F. Guerrieri, C. Limatola, M. Catalano, Microglia-derived microvesicles affect microglia phenotype in glioma, Front. Cell. Neurosci. 13 (2019) 41, https://doi.org/10.3389/fncel.2019.00041.
[7] E. Cocucci, J. Meldolesi, Ectosomes and exosomes: shedding the confusion between extracellular vesicles, Trends Cell Biol. 25 (2015) 364–372, https://doi.org/10.1016/j.tcb.2015.01.004.
[8] G. Raposo, W. Stoorvogel, Extracellular vesicles: exosomes, microvesicles, and friends, J. Cell Biol. 200 (2013) 373–383, https://doi.org/10.1083/jcb.201211138.
[9] S.L.N. Maas, X.O. Breakefield, A.M. Weaver, Extracellular vesicles: unique intercellular delivery vehicles, Trends Cell Biol. 27 (2017) 172–188, https://doi.org/10.1016/j.tcb.2016.11.003.
[10] C. Frühbeis, D. Fröhlich, E.-M. Krämer-Albers, Emerging roles of exosomes in neuron–glia communication, Front. Physiol. 3 (2012) 119, https://doi.org/10.3389/fphys.2012.00119.
[11] G. Lachenal, K. Pernet-Gallay, M. Chivet, F.J. Hemming, A. Belly, G. Bodon, B. Blot, G. Haase, Y. Goldberg, R. Sadoul, Release of exosomes from differentiated neurons and its regulation by synaptic glutamatergic activity, Mol. Cell. Neurosci. 46 (2011) 409–418, https://doi.org/10.1016/j.mcn.2010.11.004.
[12] K.E. van der Vos, L. Balaj, J. Skog, X.O. Breakefield, Brain tumor microvesicles: insights into intercellular communication in the nervous system, Cell. Mol. Neurobiol. 31 (2011) 949–959, https://doi.org/10.1007/s10571-011-9697-y.
[13] D. Ha, N. Yang, V. Nadithe, Exosomes as therapeutic drug carriers and delivery vehicles across biological membranes: current perspectives and future challenges, Acta Pharm. Sin. B. 6 (2016) 287–296, https://doi.org/10.1016/J.APSB.2016.02.001.
[14] C. Verderio, L. Muzio, E. Turola, A. Bergami, L. Novellino, F. Ruffini, L. Riganti, I. Corradini, M. Francolini, L. Garzetti, C. Maiorino, F. Servida, A. Vercelli, M. Rocca, D.D. Libera, V. Martinelli, G. Comi, G. Martino, M. Matteoli, R. Furlan, Myeloid microvesicles are a marker and therapeutic target for neuroinflammation, Ann. Neurol. 72 (2012) 610–624, https://doi.org/10.1002/ana.23627.
[15] S. EL Andaloussi, I. Mäger, X.O. Breakefield, M.J.A. Wood, Extracellular vesicles: biology and emerging therapeutic opportunities, Nat. Rev. Drug Discov. 12 (2013) 347–357, https://doi.org/10.1038/nrd3978.
[16] K.P. Loh, Q. Bao, G. Eda, M. Chhowalla, Graphene oxide as a chemically tunable platform for optical applications, Nat. Chem. 2 (2010) 1015–1024, https://doi.org/10.1038/nchem.907.
[17] G. Reina, J.M. González-Domínguez, A. Criado, E. Vázquez, A. Bianco, M. Prato, Promises, facts and challenges for graphene in biomedical applications, Chem. Soc. Rev. 46 (2017) 4400–4416, https://doi.org/10.1039/c7cs00363c.
[18] M. Baldrighi, M. Trusel, R. Tonini, S. Giordani, Carbon nanomaterials interfacing with neurons: an in vivo perspective, Front. Neurosci. 10 (2016) 250, https://doi.org/10.3389/fnins.2016.00250.
[19] R. Rauti, N. Lozano, V. León, D. Scaini, M. Musto, I. Rago, F.P. Ulloa Severino, A. Fabbro, L. Casalis, E. Vázquez, K. Kostarelos, M. Prato, L. Ballerini, Graphene oxide nanosheets reshape synaptic function in cultured brain networks, ACS Nano 10 (2016) 4459–4471, https://doi.org/10.1021/acsnano.6b00130.
[20] R. Rauti, M. Medelin, L. Newman, S. Vranic, G. Reina, A. Bianco, M. Prato, K. Kostarelos, L. Ballerini, Graphene oxide flakes tune excitatory neurotransmission in vivo by targeting hippocampal synapses, Nano Lett. 19 (2019) 2858–2870, https://doi.org/10.1021/acs.nanolett.8b04903.
[21] Z. Song, Y. Wang, Z. Xu, Mechanical responses of the bio-nano interface: a molecular dynamics study of graphene-coated lipid membrane, Theor. Appl. Mech. Lett. 5 (2015) 231–235, https://doi.org/10.1016/j.taml.2015.11.003.
[22] R.J. Rodrigues, A.R. Tomé, R.A. Cunha, ATP as a multi-target danger signal in the brain, Front. Neurosci. 9 (2015) 148, https://doi.org/10.3389/fnins.2015.00148.
[23] F. Calegari, S. Coco, E. Taverna, M. Bassetti, C. Verderio, N. Corradi, M. Matteoli, P. Rosa, A regulated secretory pathway in cultured hippocampal astrocytes, J. Biol. Chem. 274 (1999) 22539–22547.
[24] P. Hermanowicz, M. Sarna, K. Burda, H. Gabryś, AtomicJ: an open source software for analysis of force curves, Rev. Sci. Instrum. 85 (2014), 063703, https://doi.org/10.1063/1.4881683.
[25] F. D'Amico, M. Saito, F. Bencivenga, M. Marsi, A. Gessini, G. Camisasca, E. Principi, R. Cucini, S. Di Fonzo, A. Battistoni, E. Giangrisostomi, C. Masciovecchio, UV resonant Raman scattering facility at Elettra, Nucl. Instruments Methods Phys. Res. Sect. A Accel. Spectrometers, Detect. Assoc. Equip. 703 (2013) 33–37, https://doi.org/10.1016/J.NIMA.2012.11.037.
[26] A. Bignami, L.F. Eng, D. Dahl, C.T. Uyeda, Localization of the glial fibrillary acidic protein in astrocytes by immunofluorescence, Brain Res. 43 (1972) 429–435, https://doi.org/10.1016/0006-8993(72)90398-8.
[27] M. Musto, R. Rauti, A.F. Rodrigues, E. Bonechi, C. Ballerini, K. Kostarelos, L. Ballerini, 3D organotypic spinal cultures: exploring neuron and neuroglia responses upon prolonged exposure to graphene oxide, Front. Syst. Neurosci. 13 (2019) 1, https://doi.org/10.3389/fnsys.2019.00001.
[28] M. Bramini, G. Alberini, E. Colombo, M. Chiacchiaretta, M.L. DiFrancesco, J.F. Maya-Vetencourt, L. Maragliano, F. Benfenati, F. Cesca, Interfacing graphene-based materials with neural cells, Front. Syst. Neurosci. 12 (2018) 12, https://doi.org/10.3389/fnsys.2018.00012.
[29] A.B. Seabra, A.J. Paula, R. De Lima, O.L. Alves, N. Durán, Nanotoxicity of graphene and graphene oxide, Chem. Res. Toxicol. 27 (2014) 159–168, https://doi.org/10.1021/tx400385x.
[30] F. Bianco, C. Perrotta, L. Novellino, M. Francolini, L. Riganti, E. Menna, L. Saglietti, E.H. Schuchman, R. Furlan, E. Clementi, M. Matteoli, C. Verderio, Acid sphingomyelinase activity triggers microparticle release from glial cells, EMBO J. 28 (2009) 1043–1054, https://doi.org/10.1038/emboj.2009.45.

[31] E. Amaral, S. Guatimosim, C. Guatimosim, Using the fluorescent styryl dye FM1-43 to visualize synaptic vesicles exocytosis and endocytosis in motor nerve terminals, Methods Mol. Biol. (2011) 137–148, https://doi.org/10.1007/978-1-60761-950-5_8.
[32] W.J. Betz, F. Mao, C.B. Smith, Imaging exocytosis and endocytosis, Curr. Opin. Neurobiol. 6 (1996) 365–371, https://doi.org/10.1016/S0959-4388(96)80121-8.
[33] A. Brumback, J.L. Lieber, J.K. Angleson, W.J. Betz, Using FM1-43 to study neuropeptide granule dynamics and exocytosis, Methods 33 (2004) 287–294, https://doi.org/10.1016/j.ymeth.2004.01.002.
[34] Y. Yoshioka, Y. Konishi, N. Kosaka, T. Katsuda, T. Kato, T. Ochiya, Comparative marker analysis of extracellular vesicles in different human cancer types, J. Extracell. Vesicles 2 (2013), https://doi.org/10.3402/jev.v2i0.20424.
[35] R.A. Dragovic, C. Gardiner, A.S. Brooks, D.S. Tannetta, D.J.P. Ferguson, P. Hole, B. Carr, C.W.G. Redman, A.L. Harris, P.J. Dobson, P. Harrison, I.L. Sargent, Sizing and phenotyping of cellular vesicles using Nanoparticle Tracking Analysis, Nanomedicine 7 (2011) 780–788, https://doi.org/10.1016/j.nano.2011.04.003.
[36] T. Visnovitz, X. Osteikoetxea, B.W. Sódar, J. Mihály, P. Lőrincz, K.V. Vukman, E.Á. Tóth, A. Koncz, I. Székács, R. Horváth, Z. Varga, E.I. Buzás, An improved 96 well plate format lipid quantification assay for standardisation of experiments with extracellular vesicles, J. Extracell. Vesicles 8 (2019), 1565263, https://doi.org/10.1080/20013078.2019.1565263.
[37] J. Mihály, R. Deák, I.C. Szigyártó, A. Bóta, T. Beke-Somfai, Z. Varga, Characterization of extracellular vesicles by IR spectroscopy: fast and simple classification based on amide and C H stretching vibrations, Biochim. Biophys. Acta Biomembr. 1859 (2017) 459–466, https://doi.org/10.1016/j.bbamem.2016.12.005.
[38] D. Ami, F. Lavatelli, P. Rognoni, G. Palladini, S. Raimondi, S. Giorgetti, L. Monti, S.M. Doglia, A. Natalello, G. Merlini, In situ characterization of protein aggregates in human tissues affected by light chain amyloidosis: a FTIR microspectroscopy study, Sci. Rep. 6 (2016) 29096, https://doi.org/10.1038/srep29096.
[39] A. Németh, N. Orgovan, B.W. Sódar, X. Osteikoetxea, K. Pálóczi, K. Szabó-Taylor, K.V. Vukman, Á. Kittel, L. Turiák, Z. Wiener, S. Tóth, L. Drahos, K. Vékey, R. Horvath, E.I. Buzás, Antibiotic-induced release of small extracellular vesicles (exosomes) with surface-associated DNA, Sci. Rep. 7 (2017) 1–16, https://doi.org/10.1038/s41598-017-08392-1.
[40] M.Y. Sherman, A.L. Goldberg, Cellular defenses against unfolded proteins: a cell biologist thinks about neurodegenerative diseases, Neuron 29 (2001) 15–32, https://doi.org/10.1016/s0896-6273(01)00177-5.
[41] R. V Rao, D.E. Bredesen, Misfolded proteins, endoplasmic reticulum stress and neurodegeneration, Curr. Opin. Cell Biol. 16 (2004) 653–662, https://doi.org/10.1016/j.ceb.2004.09.012.
[42] D.J. Selkoe, Folding proteins in fatal ways, Nature 426 (2003) 900–904, https://doi.org/10.1038/nature02264.
[43] A. Natalello, D. Ami, S.M. Doglia, Fourier transform infrared spectroscopy of intrinsically disordered proteins: measurement procedures and data analyses, Methods Mol. Biol. (2012) 229–244, https://doi.org/10.1007/978-1-61779-927-3_16.
[44] C.J. Oldfield, A.K. Dunker, Intrinsically disordered proteins and intrinsically disordered protein regions, Annu. Rev. Biochem. 83 (2014) 553–584, https://doi.org/10.1146/annurev-biochem-072711-164947.
[45] D. V Caccamo, M.M. Herman, A. Frankfurter, C.D. Katsetos, V.P. Collins, L.J. Rubinstein, An immunohistochemical study of neuropeptides and neuronal cytoskeletal proteins in the neuroepithelial component of a spontaneous murine ovarian teratoma. Primitive neuroepithelium displays immunoreactivity for neuropeptides and neuron-associated beta-tu, Am. J. Pathol. 135 (1989) 801–813.
[46] R.C. Paolicelli, G. Bergamini, L. Rajendran, Cell-to-cell communication by extracellular vesicles: focus on microglia, Neuroscience 405 (2019) 148–157, https://doi.org/10.1016/j.neuroscience.2018.04.003.
[47] Y. Yang, A. Boza-Serrano, C.J.R. Dunning, B.H. Clausen, K.L. Lambertsen, T. Deierborg, Inflammation leads to distinct populations of extracellular vesicles from microglia, J. Neuroinflammation 15 (2018) 168, https://doi.org/10.1186/s12974-018-1204-7.
[48] F. Antonucci, E. Turola, L. Riganti, M. Caleo, M. Gabrielli, C. Perrotta, L. Novellino, E. Clementi, P. Giussani, P. Viani, M. Matteoli, C. Verderio, Microvesicles released from microglia stimulate synaptic activity via enhanced sphingolipid metabolism, EMBO J. 31 (2012) 1231–1240, https://doi.org/10.1038/emboj.2011.489.
[49] M.J. Carson, J.C. Thrash, B. Walter, The cellular response in neuroinflammation: the role of leukocytes, microglia and astrocytes in neuronal death and survival, Clin. Neurosci. Res. 6 (2006) 237–245, https://doi.org/10.1016/j.cnr.2006.09.004.
[50] M.M. Holm, J. Kaiser, M.E. Schwab, Extracellular vesicles: multimodal envoys in neural maintenance and repair, Trends Neurosci. 41 (2018) 360–372, https://doi.org/10.1016/j.tins.2018.03.006.
[51] T. Gerecsei, I. Erdődi, B. Peter, C. Hős, S. Kurunczi, I. Derényi, B. Szabó, R. Horvath, Adhesion force measurements on functionalized microbeads: an in-depth comparison of computer controlled micropipette and fluidic force microscopy, J. Colloid Interface Sci. 555 (2019) 245–253, https://doi.org/10.1016/j.jcis.2019.07.102.
[52] S. Kasas, X. Wang, H. Hirling, R. Marsault, B. Huni, A. Yersin, R. Regazzi, G. Grenningloh, B. Riederer, L. Forrò, G. Dietler, S. Catsicas, Superficial and deep changes of cellular mechanical properties following cytoskeleton disassembly, Cell Motil Cytoskeleton 62 (2005) 124–132, https://doi.org/10.1002/cm.20086.
[53] E. Norman, R.G. Cutler, R. Flannery, Y. Wang, M.P. Mattson, Plasma membrane sphingomyelin hydrolysis increases hippocampal neuron excitability by sphingosine-1-phosphate mediated mechanisms, J. Neurochem. 114 (2010) 430–439, https://doi.org/10.1111/j.1471-4159.2010.06779.x.
[54] V. Amrhein, S. Greenland, B. McShane, Scientists rise up against statistical significance, Nature 567 (2019) 305–307, https://doi.org/10.1038/d41586-019-00857-9.
[55] It's time to talk about ditching statistical significance, Nature 567 (2019), https://doi.org/10.1038/d41586-019-00874-8, 283–283.
[56] R. Frost, S. Svedhem, C. Langhammer, B. Kasemo, Graphene oxide and lipid membranes: size-dependent interactions, Langmuir 32 (2016) 2708–2717, https://doi.org/10.1021/acs.langmuir.5b03239.
[57] N. Li, Q. Zhang, S. Gao, Q. Song, R. Huang, L. Wang, L. Liu, J. Dai, M. Tang, G. Cheng, Three-dimensional graphene foam as a biocompatible and conductive scaffold for neural stem cells, Sci. Rep. 3 (2013) 1604, https://doi.org/10.1038/srep01604.
[58] M. Basso, S. Pozzi, M. Tortarolo, F. Fiordaliso, C. Bisighini, L. Pasetto, G. Spaltro, D. Lidonnici, F. Gensano, E. Battaglia, C. Bendotti, V. Bonetto, Mutant copper-zinc superoxide dismutase (SOD1) induces protein secretion pathway alterations and exosome release in astrocytes: implications for disease spreading and motor neuron pathology in amyotrophic lateral sclerosis, J. Biol. Chem. 288 (2013) 15699–15711, https://doi.org/10.1074/jbc.M112.425066.
[59] G. Wang, M. Dinkins, Q. He, G. Zhu, C. Poirier, A. Campbell, M. Mayer-Proschel, E. Bieberich, Astrocytes secrete exosomes enriched with proapoptotic ceramide and prostate apoptosis response 4 (PAR-4), J. Biol. Chem. 287 (2012) 21384–21395, https://doi.org/10.1074/jbc.M112.340513.
[60] R.-D. Gosselin, P. Meylan, I. Decosterd, Extracellular microvesicles from astrocytes contain functional glutamate transporters: regulation by protein kinase C and cell activation, Front. Cell. Neurosci. 7 (2013) 251, https://doi.org/10.3389/fncel.2013.00251.
[61] A.R. Taylor, M.B. Robinson, D.J. Gifondorwa, M. Tytell, C.E. Milligan, Regulation of heat shock protein 70 release in astrocytes: role of signaling kinases, Dev. Neurobiol. 67 (2007) 1815–1829, https://doi.org/10.1002/dneu.20559.
[62] S. Wang, F. Cesca, G. Loers, M. Schweizer, F. Buck, F. Benfenati, M. Schachner, R. Kleene, Synapsin I is an oligomannose-carrying glycoprotein, acts as an oligomannose-binding lectin, and promotes neurite outgrowth and neuronal survival when released via glia-derived exosomes, J. Neurosci. 31 (2011) 7275–7290, https://doi.org/10.1523/JNEUROSCI.6476-10.2011.
[63] H. Zhao, R. Ding, X. Zhao, Y. Li, L. Qu, H. Pei, L. Yildirimer, Z. Wu, W. Zhang, Graphene-based nanomaterials for drug and/or gene delivery, bioimaging, and tissue engineering, Drug Discov. Today 22 (2017) 1302–1317, https://doi.org/10.1016/j.drudis.2017.04.002.

# Update


## Carbon

**Volume 178, Issue , 30 June 2021, Page 824**

**DOI: https://doi.org/10.1016/j.carbon.2021.04.026**

Carbon 178 (2021) 824

Contents lists available at ScienceDirect

Carbon

journal homepage: www.elsevier.com/locate/carbon

Corrigendum

# Corrigendum to Shedding plasma membrane vesicles induced by graphene oxide nanoflakes in brain cultured astrocytes [CARBON 176 (2021) 458–469]

Mattia Musto [a], Pietro Parisse [b], Maria Pachetti [b], Christian Memo [a], Giuseppe Di Mauro [a], Belen Ballesteros [c], Neus Lozano [c], Kostas Kostarelos [c, d], Loredana Casalis [b, **], Laura Ballerini [a, *]

[a] International School for Advanced Studies (SISSA), 34136, Trieste, Italy
[b] ELETTRA Synchrotron Light Source, 34149, Basovizza, Italy
[c] Catalan Institute of Nanoscience and Nanotechnology (ICN2), Campus UAB, Bellaterra, 08193, Barcelona, Spain
[d] Nanomedicine Lab, National Graphene Institute and Faculty of Biology, Medicine & Health, The University of Manchester, Manchester, M13 9PT, United Kingdom

The authors regret that the printed version of the above article contained a number of errors. The correct and final version follows. The authors would like to apologise for any inconvenience caused.

The authors would like to make the following addition to the Acknowledgment section of the article:

The authors are grateful to Dr. Gesmi Milcovich for contributing to the recording and analyses in the AFM biomechanics measurements and related fruitful discussions.

DOI of original article: https://doi.org/10.1016/j.carbon.2021.01.142.
* Corresponding author.
** Corresponding author.
*E-mail addresses:* loredana.casalis@elettra.eu (L. Casalis), laura.ballerini@sissa.it, ballerin@sissa.it (L. Ballerini).

https://doi.org/10.1016/j.carbon.2021.04.026
0008-6223/© 2021 The Author(s). Published by Elsevier Ltd. All rights reserved.